# The subglacial geology of Wilkes Land, East Antarctica

A. R. A. Aitken[1], D. A. Young[2], F. Ferraccioli[3], P. G. Betts[4], J. S. Greenbaum[2], T. G. Richter[2], J. L. Roberts[5,6], D. D. Blankenship[2], and M. J. Siegert[7,8]

[1]School of Earth and Environment, University of Western Australia, Perth, Western Australia, Australia, [2]Institute of Geophysics, University of Texas at Austin, Austin, Texas, USA, [3]The British Antarctic Survey, Cambridge, UK, [4]School of Geosciences, Monash University, Melbourne, Victoria, Australia, [5]Australian Antarctic Division, Kingston, Tasmania, Australia, [6]Antarctic Climate and Ecosystems Cooperative Research Centre, University of Tasmania, Hobart, Tasmania, Australia, [7]Bristol Glaciology Centre, School of Geographical Sciences, University of Bristol, Bristol, UK, [8]Grantham Institute, Department of Earth Sciences and Engineering, Imperial College London, London, UK

**Abstract** Wilkes Land is a key region for studying the configuration of Gondwana and for appreciating the role of tectonic boundary conditions on East Antarctic Ice Sheet (EAIS) behavior. Despite this importance, it remains one of the largest regions on Earth where we lack a basic knowledge of geology. New magnetic, gravity, and subglacial topography data allow the region's first comprehensive geological interpretation. We map lithospheric domains and their bounding faults, including the suture between Indo-Antarctica and Australo-Antarctica. Furthermore, we image subglacial sedimentary basins, including the Aurora and Knox Subglacial Basins and the previously unknown Sabrina Subglacial Basin. Commonality of structure in magnetic, gravity, and topography data suggest that pre-EAIS tectonic features are a primary control on subglacial topography. The preservation of this relationship after glaciation suggests that these tectonic features provide topographic and basal boundary conditions that have strongly influenced the structure and evolution of the EAIS.

## 1. Introduction

Due to its remoteness and thick ice cover, the interior of Wilkes Land in East Antarctica is one of the least understood geological regions on Earth, known only from a few coastal outcrops and satellite geophysical data [*Boger*, 2011; *Fitzsimons*, 2000, 2003].

The tectonic architecture of Wilkes Land is of fundamental importance to understanding the tectonic evolution of the East Antarctic Craton. This region records the assembly and breakup of the Gondwana, Rodinia, and Columbia supercontinents and is a crucial constraint on models of the supercontinent cycle [*Boger*, 2011; *Fitzsimons*, 2000; *Harley et al.*, 2013; *White et al.*, 2013]. Tectonic architecture provides a fundamental geological template for the location and evolution of subglacial sedimentary basins and paleotopography and modern topography. Thus, the tectonic architecture of this region, especially the subglacial sedimentary basins, may play a key role in the structure and evolution of the EAIS.

The Wilkes Land ice catchments may be more vulnerable to change than other EAIS catchments. The ice sheet bed is predominantly below sea level [*Fretwell et al.*, 2013] and is subject to marine ice sheet instability. Recent satellite observations indicate significant rates of change for Wilkes Land catchments, including thinning at their seaward margins [*Pritchard et al.*, 2012] and rapid basal melt rates under their flanking ice shelves [*Rignot et al.*, 2013]. A dynamic early ice sheet [*Young et al.*, 2011] indicates large changes have occurred in this part of the EAIS in the past. Some ice sheet models [*Hill et al.*, 2007; *Pollard and DeConto*, 2013] suggest partial collapse of the Wilkes Land sector of the EAIS as recently as the warm mid-Pliocene (circa 3 Ma). This may be supported by offshore detrital sedimentary records [*Cook et al.*, 2013; *Williams et al.*, 2010]; however, interpreting these requires a good understanding of the subglacial geology [*Cook et al.*, 2013].

To resolve subglacial geology and tectonics, and to interpret the potential for geological controls on ice dynamics, we analyzed more than 100,000 line kilometers of new magnetic data (Figure 1a), gravity data (Figure 1b), and subglacial topography data (Figure 1c), collected as part of the International Collaborative Exploration of the Cryosphere through Airborne Profiling (ICECAP) project. The data are available in the
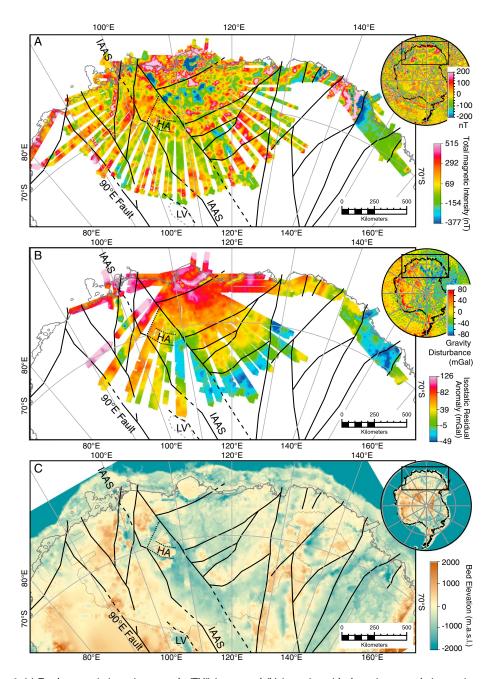
**Figure 1.** (a) Total magnetic intensity anomaly (TMI) image and (b) isostatic residual gravity anomaly image. Insets show TMI from the World Digital Magnetic Anomaly Map (WDMAM) [*Korhonen et al.*, 2007] and gravity disturbance from Eigen-6s [*Förste et al.*, 2011]. (c) Subglacial topography from ICECAP data (within grey polygon) and Bedmap-2 [*Fretwell et al.*, 2013]. Solid lines indicate observed faults, long dashed lines indicate fault segments overprinted by younger features, and short dashed lines indicate the fault-related fjords of Highland A. IAAS – Indo-Australo-Antarctic Suture; LV – Lake Vostok; and HA – Highland A.

supporting information and through the National Snow and Ice Data Center (http://nsidc.org/data/icebridge/data_summaries.html).

We identify large-scale tectonic domains based on differences in magnetic, gravity, and topographic character (Figure 3a). Although we focus on the information in our new data, our tectonic interpretations are contextualized through correlation with Australia (Figure 2). We use the fully independent "Leeuwin" Gondwana reconstruction at 160 Ma [*Williams et al.*, 2011], which provides a better fit for our new data than other recent models [*Seton et al.*, 2012; *White et al.*, 2013; *Williams et al.*, 2011]. We identify the extent and
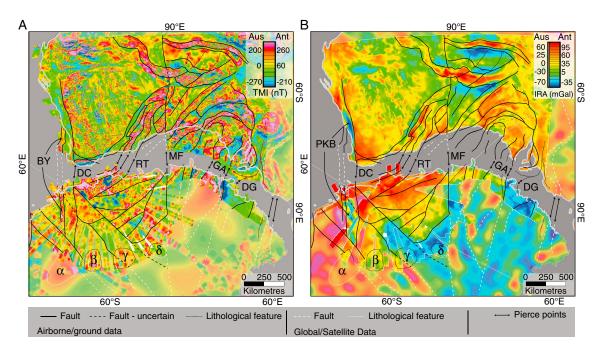
**Figure 2.** (a) Total magnetic intensity anomalies and (b) isostatic residual gravity anomalies in the Leeuwin Gondwana reconstruction at 160 Ma. The color stretch is centered on the mean value for each continent but has the same dynamic range. Interpretation also included TMI values from the EMAG2 [*Maus et al.*, 2009] (not shown) and World Digital Magnetic Anomaly Map [*Korhonen et al.*, 2007] models and gravity from the Eigen-6s satellite-only gravity model [*Förste et al.*, 2011]. Pierce points indicate regions where intercontinent correlations can be made. The major examples are BY – Bunger Hills-Yallingup Shelf; DC – Darling-Conger Fault; RT – Rodona-Totten Fault; MF – Mundrabilla-Frost Fault; GA – Gawler-Terre Adelie [*Fitzsimons*, 2003]; DG – Delamerian Granites; and PKB – Perth-Knox Basin. The $\alpha$, $\beta$, $\gamma$, and $\delta$ indicate the late granite batholiths.

estimate the thickness of overlying sedimentary basins using gravity data and depth to magnetic basement techniques (Figure 3b).

## 2. Data and Data Processing

Data processing followed methods modified from industry-standard protocols. These are briefly described below with full details in the data release notes. Interpretations outside of the new data area were constrained using Earth Magnetic Anomaly Grid 2 (EMAG2) [*Maus et al.*, 2009] and the World Digital Magnetic Map [*Korhonen et al.*, 2007] models for magnetic field, the gravity disturbance from the Eigen-6s satellite gravity model [*Förste et al.*, 2011], and subglacial topography from the Bedmap-2 compilation [*Fretwell et al.*, 2013].

### 2.1. Instrumentation

All instruments were flown aboard a Basler DC-3T aircraft fitted with the 60 MHz High Capability Radar Sounder-1 (HiCARS-1) ice-penetrating radar [see *Young et al.*, 2011], a tail-boom-mounted Geometrics G-823A cesium vapor magnetometer, and a Bell Aerospace BGM-3 two-axis stabilized scalar gravimeter. The platform also carried a laser altimeter to resolve ice-surface geometry and GPS sensors to resolve 4-D locations and aircraft accelerations.

### 2.2. Magnetic Data Processing

Magnetic data (Figure 1a) from seasons 2009–2010 through 2012–2013 were corrected for the long-term, large-scale international geomagnetic reference field and shorter time scale diurnal effects, based on observatories at Casey, Dome C, and Dumont d'Urville stations. Line data were leveled to minimize line-correlated noise. The leveled data were interpolated, using a minimum curvature method, with a cell size of 2 km as this cell size provided a good visual balance between resolution, noise, and coverage. Finally, the individual gridded data sets were merged into a single composite grid (Figure 1a).
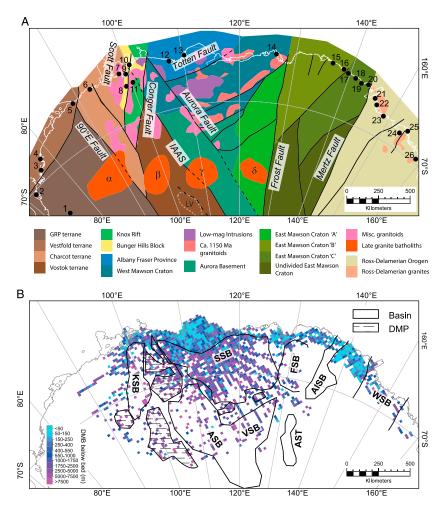
**Figure 3.** (a) Tectonic interpretation of basement geology, showing the major tectonic regions, and overprinting magmatic suites. Numbered dots indicate outcrop locations from the Antarctic Digital Database (see Table 1 for full details) key outcrops include the Prydz Bay region (1–4) [*Fitzsimons*, 2003; *Golynsky et al.*, 2006], the Bunger Hills region (7–11) [*Fitzsimons*, 2003], the Windmill Islands (13) [*Zhang et al.*, 2012], the Terre-Adelie coast (17–23) [*Fitzsimons*, 2003], and the Wilson Hills (26) [*Tessensohn and Henjes-Kunst*, 2005]. The $\alpha$, $\beta$, $\gamma$, and $\delta$ indicate the late granitoid batholiths. LV – lake Vostok. (b) Image of the depth to magnetic basement map, showing interpreted sedimentary basins. Note the distinction between inferred basins and deep magnetic provinces (DMPs); the latter typically lacking a gravity response. KSB – Knox Subglacial Basin, ASB – Aurora Subglacial Basin, SSB – Sabrina Subglacial Basin, VSB – Vincennes Subglacial Basin, FSB – Frost Subglacial Basin, AlSB – Astrolabe Subglacial Basin, AST – Adventure Subglacial Trough, and WSB – Wilkes Subglacial Basin.

## 2.3. Gravity Data Processing

Basic corrections for latitude, instrument drift, observation elevation, and the Eotvös effect, were applied to the raw data to give the gravity disturbance. For interpretation, we used the isostatic residual anomaly (IRA, Figure 1b), which has additional adjustments for glacial and subglacial topography and the depression of the crust-mantle boundary due to the ice sheet load and topographic loads. Topographic corrections used a regional 3-D model, using a density of 920 kg m$^{-3}$ for ice, 1030 kg m$^{-3}$ for seawater, and 2670 kg m$^{-3}$ for rock. The resulting Bouguer anomaly shows a slight anticorrelation with the bedrock topography (correlation coefficient ($r_{bed}$) of $-0.20$). This was essentially independent of the density of the rock layer ($r_{2720} = -0.22$; $r_{2620} = -0.18$). The ice-surface elevation showed a strong anticorrelation ($r_{surf} = -0.86$) with the Bouguer anomaly.

These anticorrelations indicate the isostatic compensation of ice, water, and rock loads. An isostatic correction was computed using the local Airy isostatic Moho depth, which varies from 45 km to 14 km, and a density contrast of 500 kg m$^{-3}$. The IRA grid was interpolated at 2 km cell size using a minimum curvature method.

**Table 1.** Rock Outcrop Locations

| Number | Name | Latitude (Approximately) | Longitude (Approximately) | Reference | Description |
|---|---|---|---|---|---|
| 1 | Grove Mountains | −72.8 | 74.7 | Fitzsimons [2003] | Prydz Complex; Cambrian Gneiss |
| 2 | Reinbolt Hills | −70.1 | 72.6 | Golynsky et al. [2006] | Neoproterozoic-Cambrian gneiss and granites |
| 3 | Larsemann Hills | −69.4 | 76.2 | Fitzsimons [2003] | Neoproterozoic-Paleozoic gneiss and granites |
| 4 | Vestfold Hills | −68.6 | 78.2 | Golynsky et al. [2006] | Archean Craton reworked in Neoproterozoic |
| 5 | Gaussberg | −66.8 | 89.1 | Sheraton and Cundari [1980] | Volcano, leucitite, late Pleistocene? |
| 6 | Mirny | −66.5 | 93.0 | Fitzsimons [2003] | Cambro-Ordovician Charnockite |
| 7 | Cape Charcot | −66.5 | 98.5 | Fitzsimons [2003] | circa 3.0 Ga tonalitic gneiss, reworked in late Neoproterozoic |
| 8 | Mount Barr-Smith and Mount Strathcona | −67.4 | 99.1 | Fitzsimons [2003] | Paragneiss |
| 9 | Obruchev Hills | −66.6 | 99.9 | Fitzsimons [2003] | Neoarchean orthogneiss, late Mesoproterozoic reworking |
| 10 | Bunger Hills | −66.3 | 100.8 | Fitzsimons [2003] | Early Mesoproterozoic orthogneiss (1.6–1.5 Ga), reworked late Mesoproterozoic (1190–1150 Ma) |
| 11 | Mount Sandow and Mount Amundsen | −67.3 | 100.5 | Fitzsimons [2003] | Folded sedimentary rocks, basalt |
| 12 | Snyder Rocks | −66.6 | 107.8 | SCAR Gazetteer | N/A |
| 13 | Windmill Islands | −66.4 | 110.6 | Zhang et al. [2012] | Early Mesoproterozoic gneiss, reworked middle (circa 1.35 Ga) and late Mesoproterozoic (1190–1100 Ma) |
| 14 | Cape Goodenough | −66.5 | 126.7 | SCAR Gazetteer | N/A |
| 15 | Mathieu Rock | 136.8 | −66.3 | SCAR Gazetteer | N/A |
| 16 | Janet Rock | −66.6 | 139.1 | SCAR Gazetteer | N/A |
| 17 | Pointe Geologie | −66.7 | 139.9 | Fitzsimons [2003] | Metasedimentary rocks and migmatite. Paleoproterozoic |
| 18 | Port Martin | −66.8 | 141.4 | Fitzsimons [2003] | Archean-paleoproterozoic gneisses |
| 19 | Cape Hunter | −67.0 | 142.3 | Fitzsimons [2003] | Phyllite; low metamorphic grade, Paleoproterozoic |
| 20 | Garnet Point | −66.9 | 143.9 | Di Vincenzo et al. [2007] and Fitzsimons [2003] | Archean-paleoproterozoic gneisses |
| 21 | Penguin Point | −67.6 | 146.0 | Di Vincenzo et al. [2007] | Cambro-Ordovician granite and schist |
| 22 | Cape Webb | −68.0 | 146.9 | Di Vincenzo et al. [2007] | Cambro-Ordovician Ma granite and schist |
| 23 | Horn Bluff | −68.4 | 148.9 | Di Vincenzo et al. [2007] | Ferrar Dolerite and Permo-Triassic Beacon Sandstone |
| 24 | Scar Bluffs | −68.8 | 153.5 | SCAR Gazetteer | N/A |
| 25 | Mawson Peninsula | −68.6 | 153.8 | SCAR Gazetteer | N/A |
| 26 | Wilson Hills | −69.7 | 158.9 | Tessensohn and Henjes-Kunst [2005] | High-grade metamorphic rocks intruded by Ross Orogen granites |

### 2.4. Subglacial Topography Determination

Subglacial topography was derived from airborne radar sounding as described in *Young et al.* [2011]. For consistency, bed topography was interpolated by kriging at 2 km resolution. Apparent cross-line differences in ice thickness average less than 50 m [*Young et al.*, 2011]; this uncertainty is well correlated with local bed roughness.

### 2.5. Depth to Magnetic Basement

The depth to magnetic basement (DMB) is commonly used as a proxy for sedimentary basin thickness where seismic data are unavailable. To estimate DMB, we applied 2-D Werner deconvolution [*Ku and Sharp*, 1983] to the magnetic line data. This approach takes advantage of the high data density and consistent sampling along flight lines. We applied three passes over the data, targeted at shallow (0.5–5 km), moderately deep (2.5–15 km), and deep (5–30 km) sources. Errors are hard to quantify but are commonly 20–40% of the source-sensor separation [*Ku and Sharp*, 1983] and so with thicker ice, greater error in estimates can be expected.

We interpolated the DMB estimates using a direct gridding method, with 20 km cells. In each cell the shallowest DMB estimate is considered the depth to magnetic basement for that cell, giving a conservative measure of potential basin thickness. Erroneously shallow DMB estimates that occur above the base of the ice sheet were rejected prior to gridding. Erroneously deep DMB estimates cannot be so easily excluded. In the better sampled regions, where several flight lines pass through each 20 km cell, these should be eliminated by the gridding process. In the poorer sampled regions, erroneously deep DMB estimates may remain. Despite significant scatter in both data sets, these DMB estimates are anticorrelated with the IRA with a correlation coefficient of $-0.282$. This accords with the expected situation where the basin is filled with relatively low-density sedimentary rocks.

## 3. Tectonic Interpretation

Interpretations presented in *Fitzsimons* [2000, 2003] and *Boger* [2011] suggest that the survey region consists of at least two and possibly three continent-scale regions. The easternmost (Australo-Antarctica) [*Fitzsimons*, 2000] has geological affinities with southern Australia, whereas the westernmost (Indo-Antarctica) [*Fitzsimons*, 2000] has geological affinities with eastern India.

*Boger* [2011] proposed an additional intervening region, the Crohn Craton. The available geophysical data over the Crohn Craton, including our new data, the Bedmap-2 compilation [*Fretwell et al.*, 2013] and recent satellite gravity models [*Förste et al.*, 2011] suggest a close affinity in lithospheric properties and structure to Indo-Antarctica. We consider this region to belong to a large composite Indo-Antarctica. We interpret one first-order continental boundary, the Indo-Australo-Antarctic Suture.

## 4. The Indo-Australo-Antarctic Suture

On geological evidence (Table 1), the suture between Australo-Antarctica and Indo-Antarctica (or the Crohn Craton) lies beneath the Denman and/or Scott Glacier(s) [*Boger*, 2011; *Fitzsimons*, 2003]. *Fitzsimons* [2003] and most subsequent interpretations propose this suture to follow a southerly route to the south of the Miller Range, passing by the Lake Vostok region [*Boger*, 2011; *Harley et al.*, 2013].

We take the suture to be defined by fundamental changes in magnetic trends, density, and topography. Using these criteria, our interpreted suture trends south-southeast from the Scott Glacier, with reasonably linear geometry, and is inferred to extend inland for over 1500 km (Figure 1). This suture is defined by the truncation of magnetic trends, which are dominantly NE in the Australo-Antarctica and SSE in Indo-Antarctica (Figure 1a), and contrasts in gravity data (Figure 1b). The suture zone also bounds the high subglacial topography of Indo-Antarctica against the low-lying topography of the Mawson Craton (Figure 1c).

## 5. Indo-Antarctica

Crustal structure to the west of the Indo-Australo-Antarctic Suture (IAAS) largely parallels the suture and may date to the collision of Indo-Antarctica with Australo-Antarctica, perhaps during the latest Mesoproterozoic and/or earliest Cambrian [*Boger*, 2011; *Collins and Pisarevsky*, 2005]. Topography is likely to have been

rejuvenated during Paleozoic to Mesozoic continental rifting and intraplate strike-slip faulting [*Ferraccioli et al.*, 2011].

Within Indo-Antarctica we define four domains: The Vestfold terrane, The Charcot terrane, the Vostok terrane, and the Gamburtsev-Ruker-Princess Elizabeth Land (GRP) terrane. The Vestfold terrane represents crust known to be similar to eastern India [*Boger*, 2011; *Fitzsimons*, 2000; *Flowerdew et al.*, 2013]. It is characterized in our data by very high magnetic anomalies (Figure 1a) and, in satellite gravity data, by high-gravity anomalies (Figure 2b). These anomalies continue to the Vestfold Hills region (Table 1, Figure 3), where high-susceptibility gneiss is associated with magnetic highs [*Golynsky et al.*, 2006]. The ice sheet bed is of lower elevation than elsewhere in Indo-Antarctica (Figure 1c).

The Charcot terrane is bounded to the west by a major fault, here named the 90°E Fault (Figure 1), and to the east by the Knox Rift. Basement to this region may outcrop at Cape Charcot (Table 1), where a circa 3 Ga tonalitic gneiss is exposed [*Fitzsimons*, 2003]. This region is characterized by low-to-moderate magnetic intensity, with a SSE oriented lineated texture, high to very high gravity anomalies and elevated topography. The Vostok terrane is unexposed but has clear geophysical differences to the Charcot terrane, being less magnetic, less dense, and with lower lying topography (Figure 1c). This terrane is bounded to the east by the IAAS and to the west by the Knox Rift and the 90°E Fault (Figure 3). The 90°E Fault may bound the Eastern Rifts of the East Antarctic Rift System, including Lake Sovetskaya and Lake 90°E [*Ferraccioli et al.*, 2011] and may be associated with Pleistocene volcanism at Gaussberg [*Sheraton and Cundari*, 1980].

*Studinger et al.* [2003] interpreted Support Office for Aerogeophysical Research (SOAR) gravity and magnetic anomaly data in the Lake Vostok region to represent a major SSE oriented crustal boundary, possibly a suture zone. The IAAS lies ~150 km to the east, suggesting either several accreted terranes or intraplate deformation at Lake Vostok. Neither ICECAP nor SOAR data are sufficiently dense for detailed tectonic interpretations. This fundamental crustal architecture was later reactivated, perhaps as part of the East Antarctic Rift causing deepening of the Lake Vostok subglacial trench system [*Ferraccioli et al.*, 2011; *Studinger et al.*, 2003].

The GRP terrane is not covered by our data but may contain the Gamburtsev Province, inland Ruker Province, and Princess Elizabeth Land Province [*Ferraccioli et al.*, 2011; *Golynsky et al.*, 2006]. The Precambrian structural trend in this region is at a high angle to the 90°E Fault and even appears to turn into it [*Ferraccioli et al.*, 2011], suggesting they predate fault motion. The Charcot and Vostok terranes may represent a composite terrane assembled during the continental collision process that culminated in collision along the IAAS.

## 6. The Knox Rift and Bunger Hills

The Charcot and Vostok terranes and part of Australo-Antarctica are overprinted by the proposed Knox Rift. This newly identified region is defined by a narrow southwest trending zone characterized by a subdued magnetic response, lower gravity anomalies, and deeper and smoother bed topography, interpreted as expressions of rifting. Inferred granitic intrusions, mostly of low relative magnetization and low relative density, are focused around the Knox Rift. Although its age is not known, the Knox Rift is correlated to the Permian-to-Cretaceous Perth Basin in Australia (Figure 2b). The Knox Rift does not appear to cross the 90°E Fault but is continuous across the IAAS, suggesting it postdates the suturing event. It is, however, of noticeably different character either side of the IAAS, with a much thicker sedimentary basin and deeper topographic depression on the Indo-Antarctic side.

The Bunger Hills Block describes a highly magnetic region that bounds the western edge of the Knox Rift. This magnetic feature is of unknown origin but could relate to magmatic processes within the Knox Rift. It is possibly continuous with a similar magnetic feature over the Yallingup Shelf, offshore Western Australia (Figure 2a).

The prevailing model for this region interprets the Bunger Hills to be a direct continuation of the Albany Fraser Province and interpreted a continuation of the Darling Fault to exist beneath the Denman Glacier [*Fitzsimons*, 2003]. Accommodating this pierce point and the Gawler-Terre-Adelie pierce point in one model has been difficult [*White et al.*, 2013, and references therein], one complication being the length excess (~180 km) of the Antarctic margin implied in *Fitzsimons* [2003] model. The revised geometry we image here for the Conger-Darling Fault, Knox Rift-Perth Basin, and Bunger Hills region largely resolves this issue, and in this case the Leeuwin model [*Williams et al.*, 2011] is adequate.

## 7. Australo-Antarctica

The Australo-Antarctic crust is quite different to Indo-Antarctica. It is dominated by low-lying topography, exhibits either very low or very high gravity, and possesses NE-N oriented magnetic trends.

Australo-Antarctica comprises several large geophysically distinct regions, which were finally assembled in the middle to late Mesoproterozoic [*Clark et al.*, 2000; *Post et al.*, 1997], prior to IAAS suturing. The region north of the Totten Glacier including the well-studied outcrops of the Windmill Islands (Table 1) has relatively robust links with the Albany Fraser Province, and we retain this name. We divide the Mawson Craton into two fundamental divisions; the East Mawson Craton describes that part of Antarctica that broadly, but imperfectly, correlates to the Gawler Craton of Australia. The West Mawson Craton comprises a region characterized by several poorly exposed and ill-correlated terranes that may have accreted onto the western margin of the East Mawson Craton during the Mesoproterozoic. Finally, the Ross-Delamerian Orogen is interpreted east of the Mertz Fault [*Di Vincenzo et al.*, 2007].

The Aurora Subglacial Basin lies to the immediate east of the IAAS and is characterized by extremely low-lying and smooth bed topography, very low gravity and very subdued, low-intensity magnetic character. The linear and 1000 km long Aurora Fault, newly defined by this survey, segments Australo-Antarctica, and forms the eastern boundary of the Aurora Subglacial Basin. These characteristics and DMB estimates lead us to propose the existence of a major fault-bounded sedimentary basin in this region, in places over 5 km thick (Figure 3b). The basement to this basin, and also part of the Vincennes Subglacial Basin (VSB), is inferred to belong to the Mawson Craton. Northwest of the ASB, Highland A [*Young et al.*, 2011] is a triangular region bounded by the Conger Fault to the west and Aurora Fault to the east. High gravity and a moderately high intensity stippled magnetic pattern with a weak NE trend suggest this region is probably part of the West Mawson Craton. Topography is generally high but heavily incised along NE and ESE oriented fjords (Figure 1c). The location and orientation of these fjords is consistent with Riedel shears developed during shearing between the IAAS and the Aurora Fault.

The Albany-Fraser Province underlies Law Dome and is exposed around the fringe, especially in the Windmill Islands [*Post et al.*, 1997; *Zhang et al.*, 2012]. This region is characterized by extremely high magnetic intensity, including strong remnant magnetizations, very high gravity, and generally elevated subglacial topography. In contrast, the West Mawson Craton is characterized by generally moderate magnetic intensity, high to very high gravity, and low-lying subglacial topography. These two regions are separated by the Totten Fault that directly underlies the Totten Glacier. The Totten Fault may be equivalent to the Australian Rodona Fault (Figure 2), which is commonly inferred to be the mid-Mesoproterozoic suture between the Albany Fraser Province and the West Mawson Craton [*Clark et al.*, 2000].

Both these regions are intruded by two magnetically distinct intrusive suites. The older suite is characterized by strong relative magnetic lows, in some cases representing reverse remnant magnetization. Intruding into this suite and also cross-cutting the Totten Fault are highly magnetic, generally NE oriented intrusions. These later intrusions are identical in character and directional trend with circa 1150 Ma granitoids that occur throughout central-southern Australia [*Aitken and Betts*, 2008].

The East Mawson Craton is divided into four zones. Zone A is bounded to the east by the Frost Fault and possesses higher magnetization, lower-gravity, and higher topography than the West Mawson Craton. The Frost Fault is a transcontinental strike-slip fault zone that extends to at least 80°S in Antarctica, and in Australia, as the Mundrabilla Fault, it extends to at least 25°S, a total length of over 3000 km (Figure 2). Zones B and C are characterized by relatively moderate gravity and generally high elevation subglacial topography, although it is incised by several troughs including the Astrolabe Subglacial Basin. Zone C is characterized by very high intensity magnetic anomalies that, on the basis of satellite magnetic data (Figure 2a) extend inland for some distance. The region to the south, between the Frost Fault and the Mertz Fault, is not covered by ICECAP data but is inferred to belong to the East Mawson Craton.

The Mertz Fault is demarcated in our new data by a dramatic change in magnetic texture and a significant reduction in gravity, as well as a transition to much lower lying subglacial topography in the Wilkes Subglacial Basin. Basement geology to the east of the Mertz Fault is inferred to represent predominantly low-grade metasedimentary rocks of Ross Orogen age [*Di Vincenzo et al.*, 2007; *Jordan et al.*, 2013; *Tessensohn and Henjes-Kunst*, 2005]. Bodies with high relative magnetizations appear to intrude the basement (Figure 1a). An arcuate magnetic lineament connecting these to Australia (DG in Figure 2) suggests that these are magnetic granites

intruded into the Ross Orogen, similar to the Delamerian Granites that intrude the Kanmantoo Group along the Coorong Shear Zone [*White et al.*, 2013]. These basement rocks are overlain by extensive Beacon Supergroup sedimentary rocks and Ferrar Dolerite sills [*Cook et al.*, 2013; *Di Vincenzo et al.*, 2007; *Ferraccioli et al.*, 2009].

## 8. Late Granite Batholiths

A remarkable feature of the aeromagnetic data set is a series of four large (200–300 km diameter), subcircular anomalies that are aligned left to right along the southern edge of the studied area (Figures 2 and 3, labeled $\alpha$, $\beta$, $\gamma$, and $\delta$). These anomalous regions apparently crosscut all faults and other intrusive suites, suggesting they are the youngest crystalline rocks present. Regions $\alpha$ and $\beta$ are associated with magnetic highs and gravity lows relative to Indo-Antarctica. Region $\gamma$ is also a magnetic high and crosscuts the IAAS. The $\gamma$ is a gravity low relative to the Indo-Antarctic Craton but a high relative to the Mawson Craton. Region $\delta$ is a relative magnetic low within the highly magnetized East Mawson Craton and a relative gravity high. None of these regions show an obvious signature in subglacial topography, suggesting they are deep seated. Sparse data do not allow unequivocal interpretation but a reasonable explanation is a series of large granitic batholiths emplaced at depth above a lithospheric-scale structure.

## 9. Sedimentary Basins

The basement rocks are overlain by several extensive sedimentary basins that are coincident with topographic subglacial basins. We define the extent of these basins using their gravity signal (Figure 1b) and depth to magnetic basement (DMB) estimates (Figure 3b). The Knox Subglacial Basin (KSB), Aurora Subglacial Basin (ASB), Vincennes Subglacial Basin (VSB), and Wilkes Subglacial Basin (WSB) all show smooth magnetic character, low gravity, and DMB estimates several kilometers below the ice sheet bed, all characteristics of deep sedimentary basins. These basins are fault bounded and mirror the geometry of the underlying tectonic architecture (Figure 3b). The KSB is confined within the narrow Knox Rift, while the ASB and VSB are much broader and are flanked by major faults including the IAAS, Aurora Fault, and Frost Fault. The WSB may represent a retro arc basin of the Ross Orogen [*Ferraccioli et al.*, 2009].

The East Mawson Craton possesses several smaller and narrow, but locally deep, sedimentary basins, including the Frost Subglacial Basin, Astrolabe Subglacial Basin, and Adventure Subglacial Trough. These are aligned along the prevailing structural trend and may be fault controlled.

Finally, our aerogeophysical data image the Sabrina Subglacial Basin (SSB), which overlies most of the West Mawson Craton. The SSB is defined by DMB estimates typically 1–3 km below the ice sheet bed (Figure 3b). Gravity in this region is reduced relative to the coastal West Mawson Craton, where the bed is interpreted as predominantly crystalline (Figure 3b). DMB estimates and the IRA are weakly anticorrelated within the SSB region, with a correlation coefficient of −0.147.

The tectonically comparable region in Australia contains the Mesozoic Bight and Cenozoic Eucla basins [*Espurt et al.*, 2012; *Hocking and Preston*, 1998]. The mostly offshore Bight Basin consists of latest Jurassic to Late Cretaceous clastic sedimentary rocks. The Bight Basin is widespread onshore but has very variable thickness, from absence to hundreds of meters [*Hocking and Preston*, 1998]. The overlying Eucla Basin, extensive onshore, is dominated by cool-water carbonates from the middle to late Eocene and an unconformably overlying Miocene sequence, with a cumulative thickness of ~500 to 750m onshore [*Hocking and Preston*, 1998]. Deposition perhaps initiated in response to the onset of fast spreading at the Southeast Indian Ridge at circa 43 Ma [*Espurt et al.*, 2012].

The Sabrina Subglacial Basin, and perhaps also the Frost, Aurora, and Vincennes Basins, may possess tectonic links to the Bight and/or Eucla Basins. Mesozoic continent breakup and subsequently the onset of fast spreading in the Eocene may have generated an inland sea (the SSB) that may have persisted up until the expansion of the EAIS at around 34 Ma [*Barrett*, 1996; *DeConto and Pollard*, 2003].

## 10. Wilkes Land Geology and the East Antarctic Ice Sheet

Full characterization of geological boundary conditions in Wilkes Land and their influence on the EAIS requires detailed work. Nevertheless, our new data provide the first opportunity to assess the role of the region's tectonic architecture in the dynamics and evolution of the EAIS in Wilkes Land.

Subglacial topography at all wavelengths is associated with tectonic controls that are also evident in the aeromagnetic and gravity maps, including fault-correlated scarps and valleys (Figure 1). At the largest scale, low-standing, smoother-surfaced regions correlate with inferred sedimentary basins and rougher-surfaced, high-standing regions correlate with inferred basement highlands. In Wilkes Land, the basins, especially the ASB and SSB, show well-distributed hydrologic systems, compared to the highlands, where flow is more focused [*Wright et al.*, 2012].

With a persistent continent-scale ice sheet, low-lying regions are inherently more susceptible to glacial activity, due to thicker ice and strong thermomechanical feedbacks between stress, deformation, and heating [e.g., *Payne and Dongelmans*, 1997]. Nevertheless, geological differences in the ice sheet bed are also important focusing mechanisms. Relevant focusing mechanisms for increased activity in the Wilkes Land basins include differences in bed roughness [e.g., *Siegert et al.*, 2004], topographic focusing in valleys [*Young et al.*, 2011], increased susceptibility to glacial erosion [e.g., *Alley*, 1993; *Kamb*, 1991], and distributed rather than focused subglacial hydrologic systems [e.g., *Schroeder et al.*, 2013; *Wright et al.*, 2012], and high geothermal flux above radiogenic granites [*Carson et al.*, 2014].

Consequently, through topographic forcing, and reinforced by the associated differences in the bed conditions, the tectonic architecture of Wilkes Land has provided persistent and strong boundary conditions on the EAIS throughout both dynamic and stable periods of ice sheet behavior.

## References

Aitken, A. R. A., and P. G. Betts (2008), High-resolution aeromagnetic data over central Australia assist Grenville-era (1300–1100 Ma) Rodinia reconstructions, *Geophys. Res. Lett.*, *35*, L01306, doi:10.1029/2007GL031563.

Alley, R. B. (1993), In search of ice-stream sticky spots, *J. Glaciol.*, *39*, 447–454.

Barrett, P. J. (1996), Antarctic Paleoenvironment through Cenozoic times—A review, *Terra Antartica*, *3*, 103–119.

Boger, S. D. (2011), Antarctica—Before and after Gondwana, *Gondwana Res.*, *19*(2), 335–371.

Carson, C. J., S. McLaren, J. L. Roberts, S. D. Boger, and D. D. Blankenship (2014), Hot rocks in a cold place: High sub-glacial heat flow in East Antarctica, *J. Geol. Soc.*, *171*(1), 9–12.

Clark, D. J., B. J. Hensen, and P. D. Kinny (2000), Geochronological constraints for a two-stage history of the Albany-Fraser Orogen Western Australia, *Precambrian Res.*, *102*, 155–183.

Collins, A. S., and S. A. Pisarevsky (2005), Amalgamating eastern Gondwana: The evolution of the Circum-Indian Orogens, *Earth Sci. Rev.*, *71*(3–4), 229–270.

Cook, C. P., et al. (2013), Dynamic behaviour of the East Antarctic ice sheet during Pliocene warmth, *Nat. Geosci.*, *6*(9), 765–769.

DeConto, R. M., and D. Pollard (2003), Rapid Cenozoic glaciation of Antarctica induced by declining atmospheric $CO_2$, *Nature*, *421*(6920), 245–249.

Di Vincenzo, G., F. Talarico, and G. Kleinschmidt (2007), An $^{40}$Ar-$^{39}$Ar investigation of the Mertz Glacier area (George V Land, Antarctica): Implications for the Ross Orogen-East Antarctic Craton relationship and Gondwana reconstructions, *Precambrian Res.*, *152*(3–4), 93–118.

Espurt, N., J. P. Callot, F. Roure, J. M. Totterdell, H. I. M. Struckmeyer, and R. Vially (2012), Transition from symmetry to asymmetry during continental rifting: An example from the Bight Basin-Terre Adélie (Australian and Antarctic conjugate margins), *Terra Nova*, *24*(3), 167–180.

Ferraccioli, F., E. Armadillo, T. Jordan, E. Bozzo, and H. Corr (2009), Aeromagnetic exploration over the East Antarctic Ice Sheet: A new view of the Wilkes Subglacial Basin, *Tectonophysics*, *478*(1–2), 62–77.

Ferraccioli, F., C. A. Finn, T. A. Jordan, R. E. Bell, L. M. Anderson, and D. Damaske (2011), East Antarctic rifting triggers uplift of the Gamburtsev Mountains, *Nature*, *479*(7373), 388–392.

Fitzsimons, I. C. W. (2000), A review of tectonic events in the East Antarctic Shield and their implications for Gondwana and earlier supercontinents, *J. Afr. Earth Sci.*, *31*(1), 3–23.

Fitzsimons, I. C. W. (2003), Proterozoic basement provinces of southern and southwestern Australia, and their correlation with Antarctica, *Geol. Soc. Spec. Publ.*, *206*, 93–130.

Flowerdew, M. J., S. Tyrrell, S. D. Boger, I. C. W. Fitzsimons, S. L. Harley, E. V. Mikhalsky, and A. P. M. Vaughan (2013), Pb isotopic domains from the Indian Ocean sector of Antarctica: Implications for past Antarctica-India connections, *Geol. Soc. Spec. Publ.*, *383*(1), 59–72.

Förste, C., et al. (2011), EIGEN-6: A new combined global gravity field model including GOCE data from the collaboration of GFZ-Potsdam and GRGS-Toulouse, *EGU General Assembly 2011*.

Fretwell, P., et al. (2013), Bedmap2: Improved ice bed, surface and thickness datasets for Antarctica, *Cryosphere*, *7*(1), 375–393.

Golynsky, A. V., V. N. Masolov, V. S. Volnukhin, and D. A. Golynsky (2006), Crustal provinces of the Prince Charles Mountains region and surrounding areas in the light of aeromagnetic data, in *Antarctica: Contributions to Global Earth Sciences*, edited by D. K. Futterer et al., pp. 83–94, Springer-Verlag, Berlin, Heidelberg, New York.

Harley, S. L., I. C. W. Fitzsimons, and Y. Zhao (2013), Antarctica and supercontinent evolution: Historical perspectives, recent advances and unresolved issues, *Geol. Soc. Spec. Publ.*, *383*(1), 1–34.

Hill, D. J., A. M. Haywood, R. C. A. Hindmarsh, and P. J. Valdes (2007), Characterizing ice sheets during the Pliocene: Evidence from data and models, in *Deep-Time Perspectives on Climate Change: Marrying the Signal From Computer Models and Biological Proxies*, edited by M. Williams, pp. 517–538, Spec. Publ. J. Geol. Soc. London, London, U. K.

Hocking, R. M., and W. A. Preston (1998), Western Australia: Phanerozoic geology and mineral resources, *AGSO J. Aust. Geol. Geophys.*, *17*(3), 245–260.

Jordan, T. A., F. Ferraccioli, E. Armadillo, and E. Bozzo (2013), Crustal architecture of the Wilkes Subglacial Basin in East Antarctica, as revealed from airborne gravity data, *Tectonophysics*, *585*, 196–206.

Kamb, B. (1991), Rheological nonlinearity and flow instability in the deforming bed mechanism of ice stream motion, *J. Geophys. Res.*, *96*, 16,585–16,595.

Korhonen, J. V., et al. (2007), *Magnetic Anomaly Map of the World; Map published by Commission for Geological Map of the World*, supported by UNESCO, 1st ed., GTK, Helsinki, Finland.

Ku, C. C., and J. A. Sharp (1983), Werner deconvolution for automated magnetic interpretation and its refinement using Marquardt's inverse modeling, *Geophysics*, *48*(6), 754–774.

Maus, S., et al. (2009), EMAG2: A 2-arc min resolution Earth Magnetic Anomaly Grid compiled from satellite, airborne, and marine magnetic measurements, *Geosyst. Geochem. Geophys.*, *10*, Q08005, doi:10.1029/2009GC002471.

Payne, A. J., and P. W. Dongelmans (1997), Self-organization in the thermomechanical flow of ice sheets, *J. Geophys. Res.*, *102*(6), 12,219–12,233.

Pollard, D., and R. M. DeConto (2013), Modeling drastic ice retreat in Antarctic Subglacial Basins GC34A-03, in *AGU Fall Meeting 2013*, edited, AGU, San Francisco, Calif.

Post, N. J., B. J. Hensen, and P. D. Kinny (1997), Two metamorphic episodes during a 1340–1180 Ma convergent tectonic event in the Windmill Islands, East Antarctica, in *Proceedings of the 7th International Symposium on Antarctic Earth Sciences*, edited by C. A. Ricci, pp. 157–161, The Antarctic Region: Geological Evolution and Processes, Terra Antartica, Siena.

Pritchard, H. D., S. R. M. Ligtenberg, H. A. Fricker, D. G. Vaughan, M. R. Van Den Broeke, and L. Padman (2012), Antarctic ice-sheet loss driven by basal melting of ice shelves, *Nature*, *484*(7395), 502–505.

Rignot, E., S. Jacobs, J. Mouginot, and B. Scheuchl (2013), Ice shelf melting around Antarctica, *Science*, *341*(6143), 266–270.

Schroeder, D. M., D. D. Blankenship, and D. A. Young (2013), Evidence for a water system transition beneath Thwaites Glacier, West Antarctica, *Proc. Natl. Acad. Sci. U.S.A.*, *110*(30), 12,225–12,228.

Seton, M., et al. (2012), Global continental and ocean basin reconstructions since 200 Ma, *Earth Sci. Rev.*, *113*(3–4), 212–270.

Sheraton, J. W., and A. Cundari (1980), Leucitites from Gaussberg, Antarctica, *Contrib. Mineral. Petrol.*, *71*(4), 417–427.

Siegert, M. J., J. Taylor, A. J. Payne, and B. Hubbard (2004), Macro-scale bed roughness of the Siple Coast ice streams in West Antarctica, *Earth Surf. Processes Landforms*, *29*(13), 1591–1596.

Studinger, M., G. D. Karner, R. E. Bell, V. Levin, C. A. Raymond, and A. A. Tikku (2003), Geophysical models for the tectonic framework of the Lake Vostok region, East Antarctica, *Earth Planet. Sci. Lett.*, *216*(4), 663–677.

Tessensohn, F., and F. Henjes-Kunst (2005), Northern Victoria Land terranes, Antarctica: Far-travelled or local products?, *Geol. Soc. Spec. Publ.*, *246*, 275–291.

White, L. T., G. M. Gibson, and G. S. Lister (2013), A reassessment of paleogeographic reconstructions of eastern Gondwana: Bringing geology back into the equation, *Gondwana Res.*, *24*(3–4), 984–998.

Williams, S. E., J. M. Whittaker, and R. D. Müller (2011), Full-fit, palinspastic reconstruction of the conjugate Australian-Antarctic margins, *Tectonics*, *30*, TC6012, doi:10.1029/2011TC002912.

Williams, T., T. van de Flierdt, S. R. Hemming, E. Chung, M. Roy, and S. L. Goldstein (2010), Evidence for iceberg armadas from East Antarctica in the Southern Ocean during the late Miocene and early Pliocene, *Earth Planet. Sci. Lett.*, *290*(3–4), 351–361.

Wright, A. P., et al. (2012), Evidence of a hydrological connection between the ice divide and ice sheet margin in the Aurora Subglacial Basin, East Antarctica, *J. Geophys. Res.*, *117*, F01033, doi:10.1029/2011JF002066.

Young, D. A., et al. (2011), A dynamic early East Antarctic Ice Sheet suggested by ice-covered fjord landscapes, *Nature*, *474*(7349), 72–75.

Zhang, S. H., Y. Zhao, X. C. Liu, Y. S. Liu, K. J. Hou, C. F. Li, and H. Ye (2012), U-Pb geochronology and geochemistry of the bedrocks and moraine sediments from the Windmill Islands: Implications for Proterozoic evolution of East Antarctica, *Precambrian Res.*, *206–207*, 52–71.